Numerical and Experimental Analysis of Rotating Backward Extrusion as a New SPD Process

Xin Che[1] · Qiang Wang[1] · Beibei Dong[1] · Mu Meng[1] · Zhiming Zhang[1]

Abstract

Rotating backward extrusion (RBE) as a new severe plastic deformation technique is a continuous process to produce cylindrical tubes with fine grains and superior properties. In this study, the RBE process with an open punch was applied to the AZ80 alloy at 653 K, and the deformation mechanisms and the microstructure evolution were examined by the finite element method (FEM) and thermal simulation experiment. The results showed that the effective strain of the RBE process was higher than that of the conventional backward extrusion (CBE) process, and the strain increased with revolutions increasing. The strain improvement of the RBE process was related to the large cumulative plastic deformation imposed by the continuous rotation of the open punch. Furthermore, the extrusion load was reduced significantly in the RBE process comparing with the CBE process, due to the change of friction stress and stress state of the materials. And the maximum load reduction of the FEM and experiment was 47.33% and 31.6%, respectively. The average grain size of the RBE sample could be reduced by up to 90% in the region A at 30 N compared with the CBE sample. The maximum increase in microhardness of the RBE sample relative to the CBE sample was 23% at 30 N in the region A. Therefore, the grain refinement and mechanical properties of the materials can be substantially improved by the RBE process.

Keywords Severe plastic deformation · Rotating backward extrusion · AZ80 alloy · Finite element analysis · Microstructure

1 Introduction

Severe plastic deformation (SPD) processing is capable of producing workpieces within the grain size of submicrometer or nanometer by imposing large strain, whereas the conventional methods may refine the grains to sizes of several micrometers [1, 2]. Therefore the mechanical properties of samples processed by SPD will be improved remarkably according to Hall–Patch relationship. Nowadays, the most widely used SPD processes are equal channel angular pressing (ECAP) [3–5], accumulated roll bonding (ARB) [6, 7] and high pressure torsion (HPT) [8, 9]. However, in the above three processes, both ECAP and ARB need multipass deformation to achieve grain refinement, which is labor intensive and time consuming. Although the HPT only needs one-pass deformation, it can only be used to produce small size thin plates, which limits its industrial application.

The limitation of SPD methods mentioned above can be solved or improved by the combination processes. These combined methods can apply more effective strain to the materials and have features derived from each simple technique. The rotating extrusion (RE) process combined the torsion and extrusion is one of the SPD processes for producing ultrafine-grained (UFG) materials [10]. This processing is characterized by adding the torsion to the extrusion processes to introduce a very large shear strain into the materials. Thus, the UFG structures and the very favorable mechanical properties can be obtained, which is an important advantage of this technique. Korbel et al. [11–14] has designed a new RE deformation method called the "KOBO" method. It can introduce the cyclic shear strain to the materials by continuously changing the rotation direction of the die. Consequently, there is a permanent destabilization of the structure and the dominance of localized plastic flow in the intersecting shear bands. In addition, the extrusion force of the RE processing can be drastically decreased

✉ Qiang Wang
  nucwangqiang@163.com

1   College of Materials Science and Engineering,
    North University of China, Taiyuan 030051,
    People's Republic of China

comparing with the conventional extrusion, which is another advantage of the RE process. Kong et al. [15] has investigated the RE process and found that increasing the rotating speed and decreasing the rotating frequency of the die can effectively increase the reduction of extrusion force. Ma et al. [16, 17] has proposed that the reduction of extrusion force in the RE process can be attributed to the change of interficial friction stress and the primary stress state within the materials. However, one problem with the RE process is that not all rotary work can be transferred into the materials, which is due to the relative slippage at the interface between the rotating die and billet. And this shortcoming will reduce the production efficiency of the RE process and hinder its industrial applications.

In the present paper, a novel SPD method named rotating backward extrusion (RBE) with the possibility of producing cylindrical tubes is studied [18, 19]. Figure 1 illustrates the schematic of the RBE process. Different from the conventional backward extrusion (CBE) die structure, an open punch with transverse groove at the end face and a moveable die with longitudinal groove in the inner wall is provided, as shown in Fig. 1a. The open punch structure can increase the efficiency of torque transfer from the punch to the billet, which may not only improve the grain refinement and mechanical properties of the alloys but actually compensate for the defect of the relative slippage between the die and the billet in the RE process. To demonstrate the capability and applicability of the process, the deformation mechanisms and microstructure evolution of the AZ80 magnesium alloy processed by the CBE and RBE process are investigated by the finite element method (FEM) simulation and physical experimental analysis.

2 Principle of the RBE Process

A schematic illustrations of the RBE process is shown in the Fig. 1, the die setup consists of two main parts of the rotating open punch and the moveable die. The RBE process is performed based on the combination of the CBE and the torsion. In the CBE process, the billet has been initially placed in the die, and then with the pressure of the punch, the material is compressed and flowed through the gap between punch and die. However, in the RBE process, at first, the moveable die is needed to be moved a certain distance so that the transverse groove of the open punch can be filled with the metal, as indicated by white circle in Fig. 1b. Then the open punch begins to rotate with the moveable die continuous moving. Finally a cylindrical tube is produced from the initial billet. The open punch structure of the RBE process helps the metal flow easily and applies more shear deformation to the billet, thus the billet can obtain more strain than the CBE process.

3 Experimental Procedure

3.1 Material and Extrusion Process

In the present work, a commercial AZ80 (Mg–8.40Al–0.53Zn–0.06Mn, wt%) magnesium alloy was employed. And a cylindrical billet with a diameter of 22 mm and a length of 25 mm was machined from the as-cast ingot and then homogenized at 688 K for 16 h to eliminate the dendrite segregation and porosity in the cast structure. Figure 2a illustrates the die setup of the RBE process including the rotating open punch and the moveable die manufactured from H13 hot-working die steel and hardened to 50
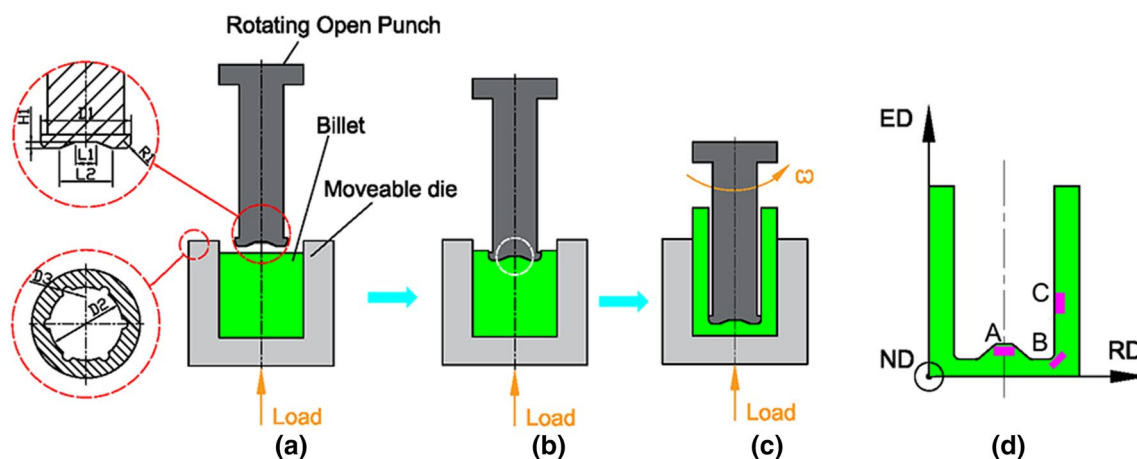

Fig. 1 Schematics of the RBE process: **a** the initial state; **b** the rotating open punch penetrating the billet; **c** the final state; **d** the processed tube and the observed position for microstructure
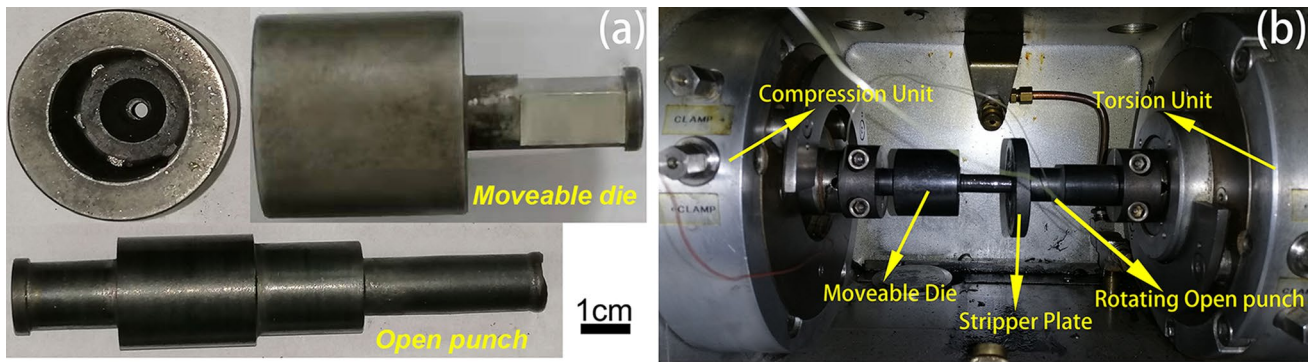
Fig. 2 **a** The die and **b** the experiment setup of the RBE process

HRC. The experiment setup including assembled die on the Gleeble-3500 thermal simulation test machine was shown in Fig. 2b. The experiment was performed at 653 K with a die speed of 0.05 mm/s. An oil-based graphite was used on the billet surface and the inner wall of the die to reduce the friction between the billet and die. The total stroke of the moveable die was 22 mm, first it was needed to move 2 mm to make the metal flow into the groove of the open punch, and then continue to move with the rotation of the open punch until the end of the stroke. Finally, the sample was needed to be quenched into water immediately to preserve deformation microstructure. The rotating speeds of the open punch are 0 (equals to the CBE process), 0.079, 0.157, 0.471, 0.785 and 1.57 rad/s, respectively, corresponding to 0 N, 5 N, 10 N, 30 N, 50 N and 100 N, i.e. the total numbers of rotating revolutions.

3.2 Microstructure Observation

The metallographic observation sample was taken from the longitudinal section of the center of the deformed tube (shown in Fig. 1d), mechanically polished and etched with the chemical reagent (0.3 g oxalic acid, 3 ml acetic acid, 20 ml distilled water). Then the obtained microstructure was examined by the optical microscope (OM, Zeiss Axio Imager-A2m, Germany). And the grain size was calculated by a software of Image-Pro Plus 6.0. The phase analysis of the extruded samples was conducted on the X-ray diffractometer (XRD, SmartLab-SE, Japan) with a Cu-Ka radiation ($\lambda = 0.154$ nm) operated at 40 kV and 40 mA with a 2θ range of 20°–80°. The Vickers microhardness (HV, VMH-002VM, Germany) was measured under the load of 200 gf for 15 s, and 10 points were tested at each position.

3.3 FEM Simulation

The DEFORM 3D-V12.0 software had been performed to analyse the deformation behavior of the AZ80 alloy during the CBE and RBE process. The main simulation parameters were given in Table 1. The data of the true stress–strain of AZ80 alloy based on the compression test [20] was entered to the material library. The geometrical dimensions of the die component and the specimens in the simulation were identical to the experiment. The material model was defined as elastic–plastic body and the die part was considered as rigid body. The relative element type was used with a initial mesh number of 50,000. The Von-Mises criterion was adapted for yielding simulation and the frictional condition was considered by the Coulomb friction model with a friction factor of 0.3. The global remeshing was chosen and the type of interference depth was selected as relative with a value of 0.7. Furthermore, the Conjugate-Gradient had been chosen as the solver of the simulation. The Craft-Latham damage criterion had been used to predict the chance of crack initiation [21].

4 Results and Discussion

4.1 FEM Analysis

The metal flow vector of the 0 N and the 30 N sample from three different views as shown in Fig. 3. It can be observed from the Fig. 3a, d that the metal of the 0 N sample mainly flows along the radial direction (RD), but the metal of the

Table 1 The utilized data for numerical simulation

Simulation data	Parameters
Initial temperature (K)	653
Die displacement (mm)	22
Rotating speed (rad/s)	0, 0.079, 0.157, 0.471, 0.785, 1.57
Die speed (mm/s)	0.05

Fig. 3 The metal flow vector of **a–c** 0 N sample and **d–f** 30 N sample
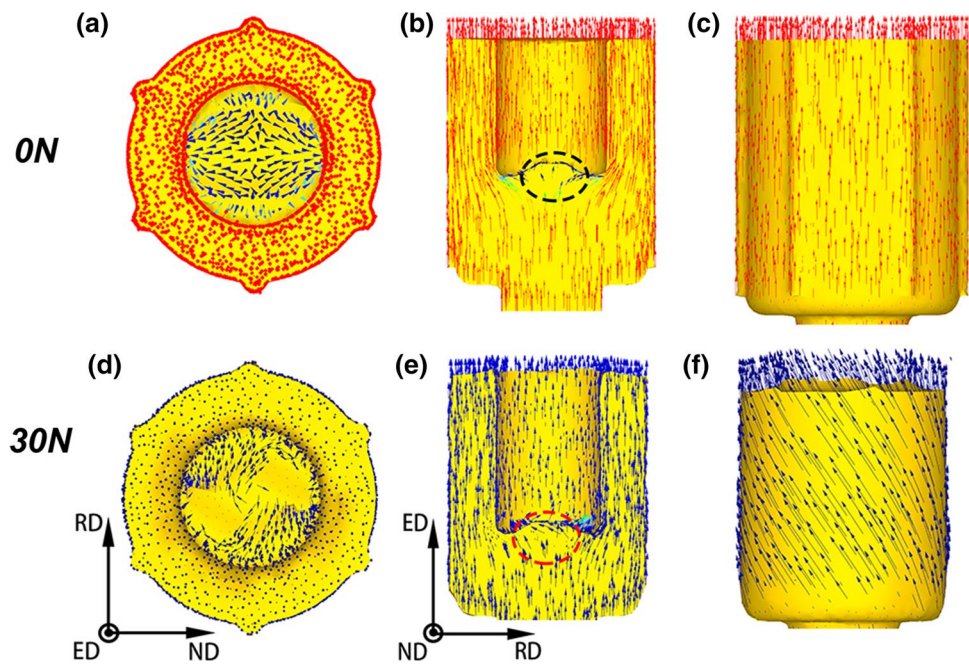
30 N sample flows along the circumferential direction around the center of the billet. It should be noted that there is a dead metal zone where the distribution of metal flow vector is sparse in the 0 N sample (indicated by the black circle in Fig. 3b), which indicates the metal fluidity in this region is poor. However, it is disappeared in the 30 N sample (indicated by the red circle in Fig. 3e). This phenomenon manifests that the RBE process can promote the metal flows more easily. The Fig. 3c, f shows the metal flow vector on the radial direction–extrusion direction (RD–ED) plane. It is observed that the metal flow trajectory of the 0 N sample is parallel to the extrusion direction, and the metal flow trajectory of the 30 N sample shows a spiral shape with about 45° from the ED. The metal flow results of the RBE process shows that the torsional effect caused by the rotation of the open punch can be transmitted from the inner wall to the outer wall of the tube sample, thereby increasing the deformation uniformity of the whole sample. Furthermore, it also can be observed from the metal flow results that the biggest difference between the RBE process and CBE process is that the additional rotation deformation is introduced to the RBE process, which completely changes the metal flow direction relative to the CBE process, and thus affects the strain distribution and the microstructure evolution of the material.

Figure 4 shows the effective strain distribution of the sample processed by the CBE and RBE process. The effective strain value is increased dramatically with the revolutions increase, and the average effective strain value of the 100 N sample is about 60 times more than that of the 0 N sample (Fig. 4b). In addition, the strain of the inner wall is higher than that of the outer wall both in the CBE and RBE

samples (Fig. 4a), which is the typical deformation characteristic of the backward extrusion. Furthermore, it can be seen from the Fig. 4a that the color between the inner and outer wall of the tube samples becomes more close with the rotating revolutions increasing, which suggests that the strain difference between the inner and outer wall is reduced and the deformation uniformity is improved. Moreover, the region where the billet is contacted with the punch has the smallest strain value in the entire billet for the 0 N sample (as indicated by the red dot circle in Fig. 4a). However, for the RBE samples, the effective strain in this region has increased drastically (as indicated by the black dot circle in Fig. 4a). And the strain value in this region has became the largest over the entire billet when the number of revolutions is more than 10 N. It can be inferred from the FEM results that comparing with the CBE process, the RBE process can substantially improve the average effective strain and the deformation uniformity, and eliminate the dead metal zone existed in the CBE process. This phenomenon may be attributed to the combined effect of the torsion and extrusion in the RBE process, which applies a more severe and uniform plastic deformation to the billet. Thus, a larger effective strain can be obtained in the RBE process compared with the CBE process. It has been reported that the large plastic deformation can effectively refine grains and improve mechanical properties of the materials [22, 23]. Therefore, the RBE process is expected to be able to produce UFG materials with excellent strength. And the effect of the RBE process on the microstructure and properties of the AZ80 alloys will be discussed in the next section.
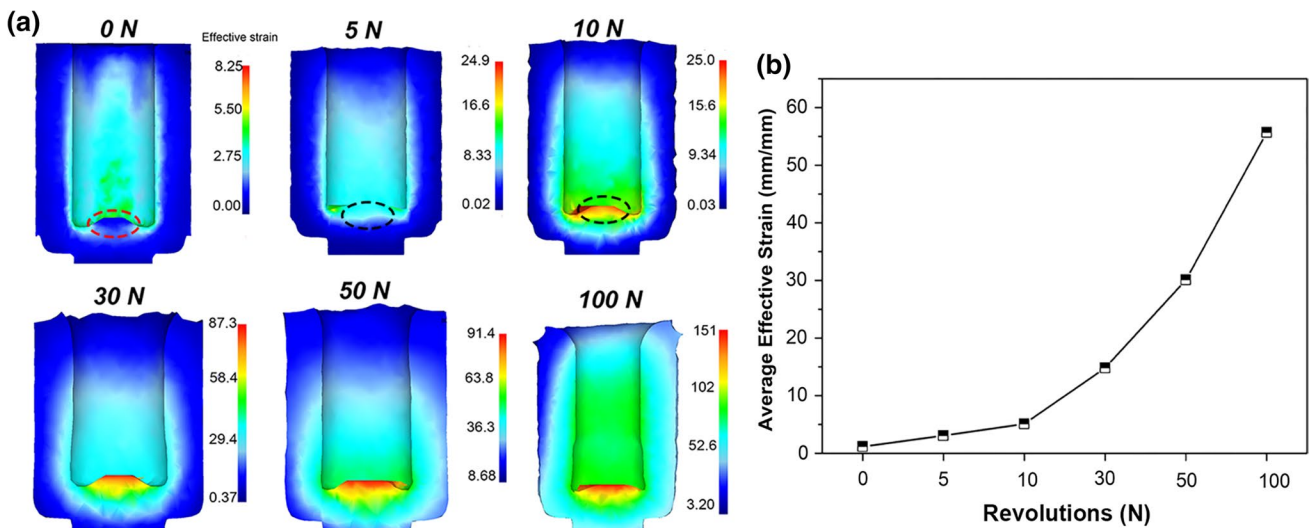
Fig. 4 **a** The effective strain distribution map and **b** the average effective strain of the CBE and RBE samples. (For interpretation of the references to colour in this figure legend, the reader is referred to the Web version of this article)

Figure 5a shows the effective strain distribution of the inner wall of the CBE and RBE samples. It can be seen from the Fig. 5a that there is a significant difference in the strain distribution of the inner wall for the CBE and RBE samples. The strain distribution of the inner wall of the 0 N sample exhibits an "M" shape, which has the lowest strain value at the bottom center of the tube (indicated by C) and the largest strain value at the shear deformation region (indicated by B and D). And, the strain gradually decreases from the bottom to the top along the tube wall (from B and D to A and E, respectively). For the 5 N sample, the "M" shape has gradually weakened and the effective strain difference between the point C and B is reduced. When the number of revolutions is greater than 10 N, the strain distribution of the inner wall changes from the "M" shape to the "A" shape, that is, the effective strain value of the point C is greater than that of the point B and D. And the strain value at the bottom center of the inner wall has became the maximum value compared to other regions. Furthermore, the strain value at the point C

of the 100 N sample is approximately 150 times more than that of the 0 N sample. Consequently, it can be deduced that the introduction of the additional rotation deformation can effectively increase the effective strain value of the tube bottom and eliminate the deformation dead zone.

Figure 5b shows the reduction in strain of the outer wall relative to the inner wall. It can be observed that the variety trend of the strain difference for the three different regions is similar, and the strain difference is first increased and then decreased with the increasing rotating revolutions. In the 0 N sample, the strain difference in the region M is the smallest because it belongs to the deformation dead zone. But, for the samples with lower rotating revolutions, the strain difference of the region M is increased drastically, which is due to only the inner wall is subjected to the additional shear deformation imposed by the punch rotation. And the maximum percentage of the strain reduction can be obtained in the 5 N sample with 96.10% at the region O. Moreover, the large strain difference between the inner and outer wall

Fig. 5 **a** The effective strain of the inner wall of the tube for all samples and **b** the percentage of effective strain reduction of the outer wall relative to the inner wall of the tube samples
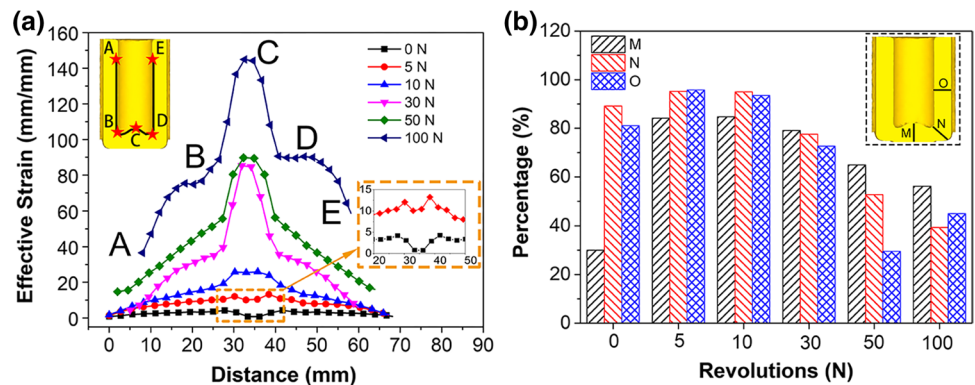
at the lower revolutions can be attributed to that the strain of the inner wall increases rapidly, while the strain of the outer wall is not changed significantly. However, with the rotating revolutions increase, more shear deformation can be transmitted from the inner wall to the outer wall, so the strain difference is reduced, and the minimum percentage of the reduction is about 31.06% at the region O in the 50 N sample. Therefore, it can be inferred that the RBE process can improve the uniformity of deformation, but it needs to reach the critical rotating revolutions, which is related to the geometry size of the mold structure and the processing parameters of the deformation.

Figure 6 shows the point tracking map of the 0 N sample and 50 N sample. It can be observed from the 0 N sample

(Fig. 6b) that the P1, P3 and P4 are located at the tube bottom where the effective strain value is pretty small and the P2, P5 and P6 are flowed into the inner wall. However, for the 50 N sample (Fig. 6c), all points are flowed into the tube wall except the P5 is still stayed at the tube bottom. It also should be noted that the effective strain of the 50 N sample is higher than that of the 0 N sample especially in the tube bottom. And it can be inferred that the RBE process can effectively improve the metal fluidity of the materials, especially at the tube bottom.

Figure 7 shows the effective strain and strain rate of the selected nodes (Fig. 6) versus the die displacement of the 0 N and 50 N samples. It can be observed from the Fig. 7a that the effective strain value of the P2 and P6 is quickly

Fig. 6 The point tracking map of **a** initial state, **b** 0 N sample and **c** 50 N sample
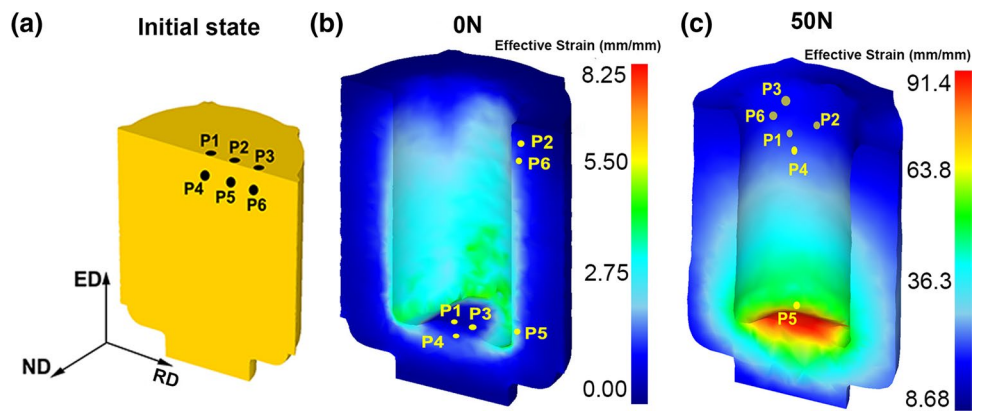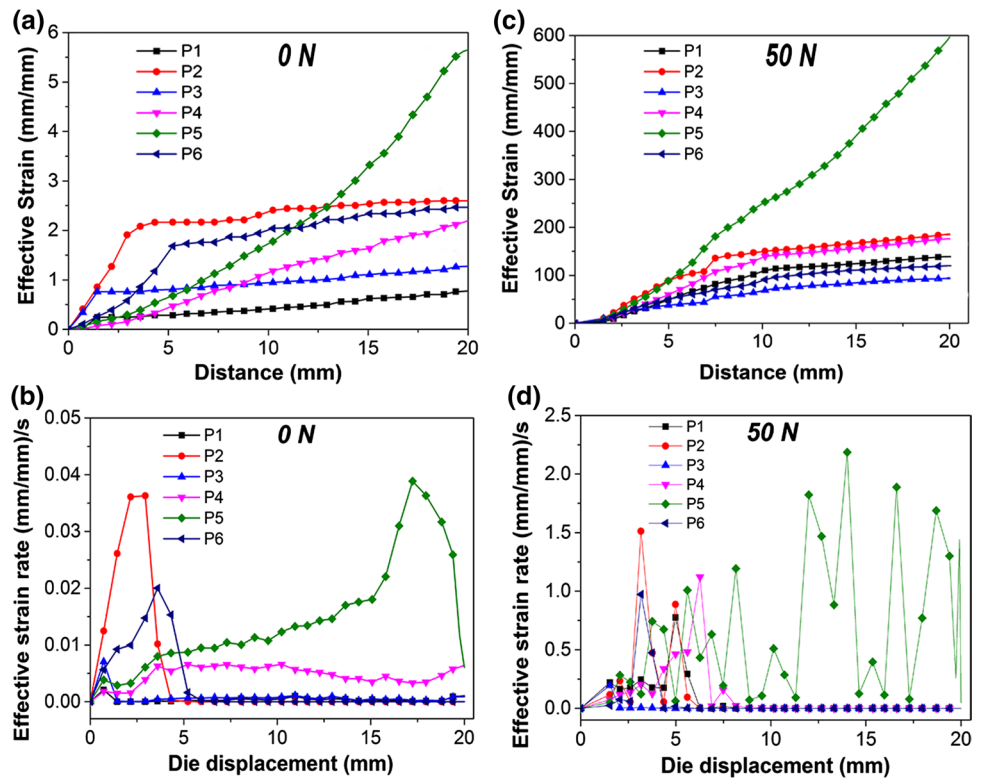

Fig. 7 The effective strain and effective strain rate of the selected nodes in Fig. 6: **a**, **b** 0 N sample and **c**, **d** 50 N sample

reached the peak strain due to the effect of the shear strain imposed by the reverse metal flow, then the strain value is not changed anymore. And the strain value of the P5 is increased gradually with the die displacement increasing. However, for the 50 N sample (Fig. 7c), the variety trend of the effective strain value of the P1–P6 is similar except that the strain value of the P5 is significantly larger than others, due to only the P5 is still located at the tube bottom after deformation (Fig. 6c). The above strain trend of the CBE and RBE samples can be further explained by the corresponding variety trend of the effective strain rate. It can be seen from the Fig. 7b that the effective strain rate of the P1, P3 and P4 in the 0 N sample are almost a straight line with no obvious peaks. However, there is clearly one peak appearing in P1, P5 and P6, respectively, which indicates the strain has occurred. The Fig. 7d shows that the effective strain rate curve of the 50 N sample is wavy and has multiple peaks, which means that the repeated plastic deformation is occurred during the RBE process. Particularly, the strain rate trend of the P5 has the most peaks and its fluctuation amplitude is also the largest, which is the reason why its effective strain value is the largest compared with other nodes. The variety trend of the effective strain rate of the 50 N sample also demonstrates that the large accumulative plastic strain can be applied to the materials by continuous rotation of the open punch.

Figure 8 shows the metal flow trajectory of the P5 on the ND-RD plane for the 0 N and 50 N samples. It can be observed from the Fig. 8a that the P5 only moves about 2.7 mm along the RD, while has almost no displacement along the ND for the 0 N sample. However, the metal flow trajectory of the 50 N sample is completely different from the 0 N sample, and the P5 makes an approximate circular motion around the center of the ND–RD plane. It also should be noted that the 50 N sample has more metal flow distance than 0 N sample. Therefore, it can be inferred that the RBE sample can obtain a larger strain compared with the CBE sample due to the billet will be subjected to continuous severe deformation caused by the additional rotation. Furthermore, it is because of the enhancement of the metal

fluidity in the RBE process that the deformation dead zone existed in the CBE process has been eliminated. Thus, the strain difference between the top and the bottom of the tubes is reduced, which means the deformation uniformity is substantially improved.

Figure 9 shows a diagram of the damage distribution of the CBE and RBE samples. The damage value is increased with the rotating revolutions increasing. It can be seen from the simulation results shown in the Fig. 9 that the damage including wrinkles and cracks are mainly occurred at the top of the tube samples both in 50 N and 100 N samples. This may be because when the rotational speed exceeds a critical value, the billet will be subjected to a high centrifugal force. And, since the upper part of the tube samples is not restricted by the mold, thus it will expand outward and gradually cause defects such as cracks and wrinkles. Therefore, it should be noted that the RBE process cannot be carried out at higher revolutions to avoid the occurrence of defects, although a higher strain can be obtained.

It can be seen from the Fig. 10a, b that all samples have similar load change trends for the FEM and experiments. And the extrusion load of the RBE samples is obviously lower than that of CBE samples both in the simulation and
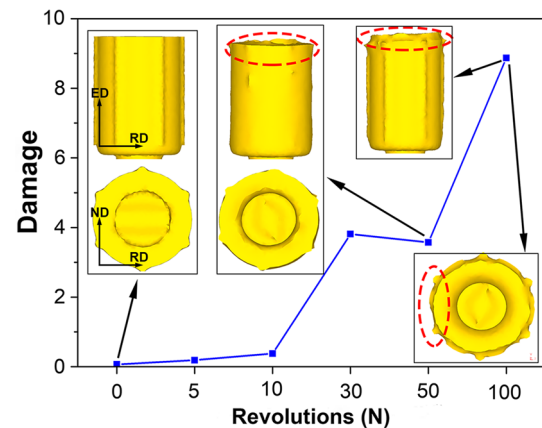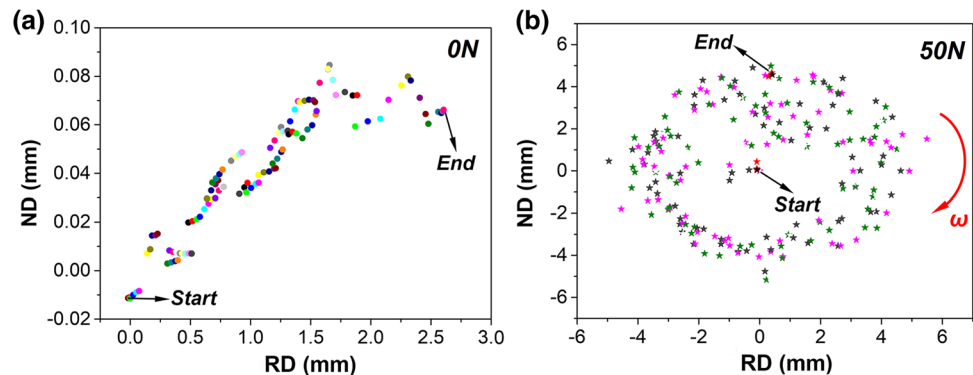
Fig. 9 The damage distribution of the CBE and RBE samples (the corresponding FEM results are embedded in the figure)

Fig. 8 The metal flow trajectory of the P5 selected in the Fig. 6 of **a** 0 N sample and **b** 50 N sample on the ND–RD plane
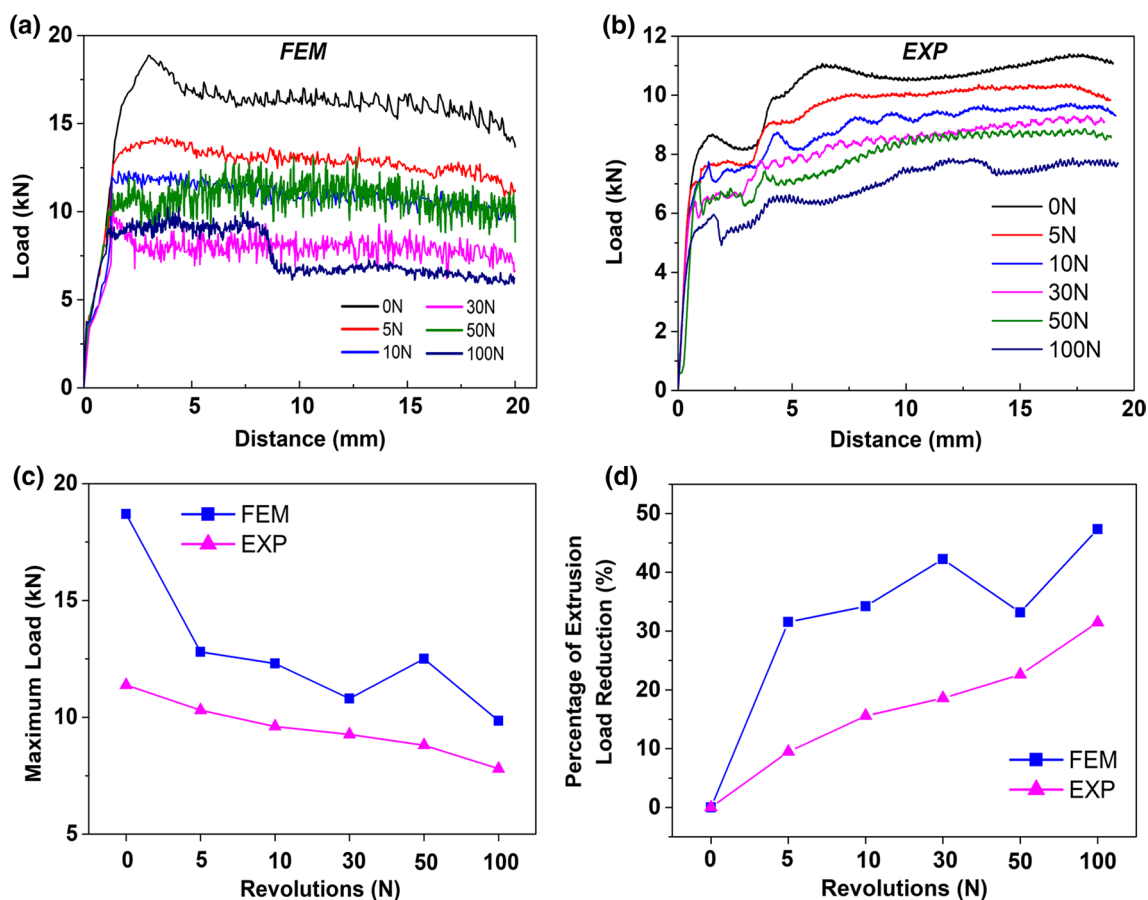
Fig. 10 The Load-Stroke curves of the **a** FEM and **b** experiment; **c** the comparison of the maximum load of simulation and experimental investigation for the CBE and RBE samples; **d** the effect of rotating revolutions on the extrusion load reduction

experimental results, which is similar to the investigation of Kobel et al. [14] and Ma et al. [16, 17]. Furthermore, it also should be noted that the load of 50 N sample is similar to that of 10 N sample in the FEM results (Fig. 10a). This may be due to the excessively high rotational speed will reduce the centering of the billet and the die, resulting a sharp increase of the extrusion load. Figure 10c shows that the extrusion load decreases with rotating revolutions

increasing, and the load of experiment results is lower than that of the FEM simulation results. By comparing the results of simulation and experiment, it can be seen that there is no obvious defects in the appearance of the physical experimental samples (Fig. 11), while the samples in the simulation results show a large damage value at the higher rotating revolutions (indicated by red dot circles in Fig. 9). Therefore, the extrusion load of experiment is smaller than that of the

Fig. 11 The processed tube samples of the CBE and RBE process
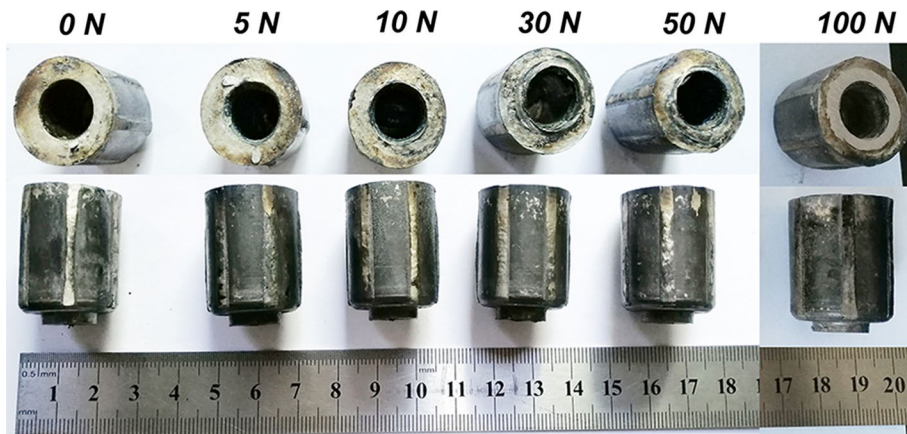
simulation results. Furthermore, the difference between simulation and experimental investigation may also be related to the material constitutive models in the FEM simulation and the actual friction conditions of the physical experiment.

Figure 10d shows the percentage of extrusion load reduction of the RBE sample relative to the CBE sample for FEM simulation and physical experiment. The percentage of load reduction increases as the rotating revolutions increases both in the FEM simulation and experiment results, and the maximum reduction of the simulation and experimental results can reach 47.33% and 31.48% respectively in the 100 N sample. The observation infers that the load of the RBE process is sensitive to the rotating speed. Ma et al. [17] had proposed two reasons for the load reduction of the RE process: (1) The rotation of the punch changed the direction of the interfacial friction stress from the original direction, which transformed part of the inactive friction into the active friction and ultimately reduced the extrusion load. (2) The stress state of the billet was changed from a compressive stress to a combined stress containing the shear stress and compressive stress, thus the primary stress of the material

was reduced according to the yield criterion, which finally caused the load reduction. In addition, the efficiency of the load reduction is related to the mold design and deformation parameters. And, increasing the rotation speed and the friction stress between the die and billet may also be an effective way to promote the load reduction.

4.2 Microstructure Observation

Figure 12 shows the optical microstructure of the CBE and RBE samples. It can be observed that the change of grain size at the region A is the most drastic among three regions (Fig. 12a, d and g). The average grain size first decreases from about 90 μm of the 0 N sample to about 11.26 μm of the 30 N sample, and then increases to 18.68 μm of the 100 N at the region A. But the difference of grain size between the CBE and RBE samples are small at both region B and region C. Thus, the region A where the punch contacts with the billet is the most severe plastic deformation region during the RBE process, which is corresponded to the effective strain of the FEM results (shown in Fig. 3a).
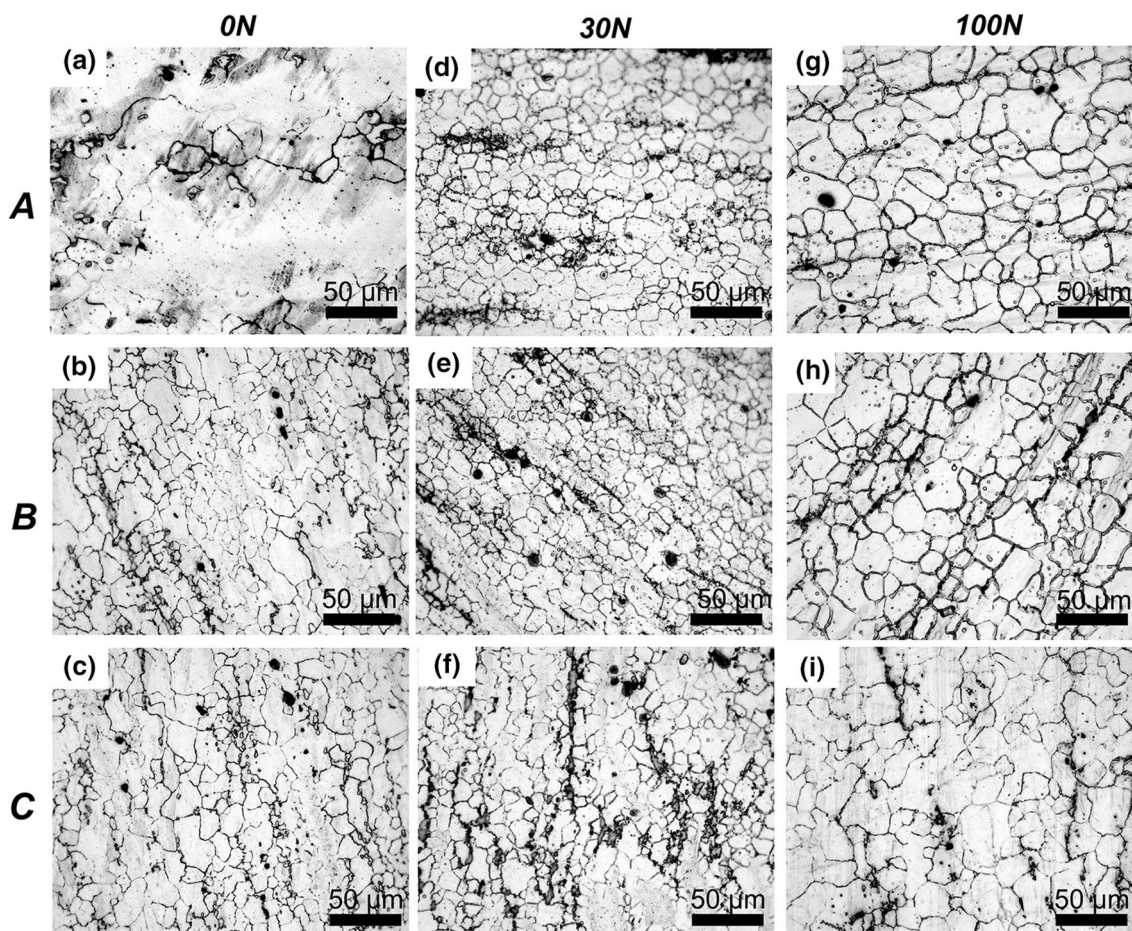

Fig. 12 The OM images at three different regions of **a–c** 0 N, **d–f** 30 N and **g–i** 100 N samples (the regions were indicated in the Fig. 1d)

Furthermore, it should be noted that the grain size difference between the three regions of the RBE samples is smaller than that of the CBE sample. Thus, it can be inferred that the RBE process can effectively refine grains and improve the deformation uniformity of materials comparing with the CBE process.

Figure 13 is the XRD results of the studied alloy at both CBE and RBE process. It can be observed that the composition of AZ80 alloy is mainly composed of α-Mg matrix and β-$Mg_{17}Al_{12}$ phase and has no obvious change among CBE and RBE samples.

Figure 14a illustrates the average grain size of the CBE and RBE samples at the regions A–C. It can be seen that the average grain size of the three regions reaches a minimum at 30 N, then it gradually grows as the rotating revolutions increasing. And the average grain size can be reduced by up to 90% at 30 N compared with the 0 N in the region A. This trend is similar to the results of other SPD investigations [24]. It is reported that there is a critical grain size in the SPD process, that is, when the strain reaches the limit value, even if the strain continues to increase, the grain size of the

alloy will not be refined anymore [25–28]. The critical grain size, in the processing of distinct metals and alloys, relates to the hydrostatic pressure, strain path, stacking faults energy, purity level, strain rate, and the deformation temperature [29]. Moreover, the saturation of grain size can be decreased significantly by reducing the deformation temperature [29] and increasing the hydrostatic pressure [30]. Therefore, it is possible to improve the grain refinement ability of the RBE process from the above methods. It is also noted that the average grain size of the region A is larger than that of the region B and C, and the grain size of the region C is slightly higher than that of the region B. This is because the region B has a shear strain formed by the reverse metal flow, so that the grain size has been further refined. Furthermore, the grain size of the region C is slightly larger than that of the region B. It may be attributed to the frictional heat, which can make grains grow rapidly.

The microhardness changes of the CBE and RBE samples at the three regions are shown in Fig. 14b. For the region A, the microhardness value of the RBE samples is higher than that of the CBE sample. The maximum value is obtained in the 30 N sample with about 95 HV, which increases by nearly 23% over the value of the 0 N sample. And the trend of microhardness in the region A is opposite to that of the grain size change. It is known that the microhardness value can indirectly represent the resistance ability to plastic deformation of the materials. Furthermore, the grain boundary can hinder the dislocation motion and increase the microhardness value. The refined grains with complex grain boundaries are more inclined to hinder dislocation motion, which will lead a higher microhardness value [31]. Therefore, it is reasonable to believe that the RBE process can not refine the grains but improve the mechanical properties of the materials. In addition, in the region B and C, the microhardness reaches a maximum of 86.4 HV and 84.9 HV at 50 N respectively, although the grain size of the 50 N sample is not the smallest. The results indicate that the microhardness may also be related to the dynamic precipitation and the
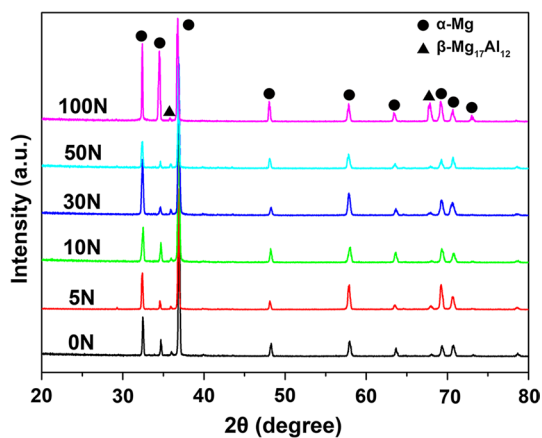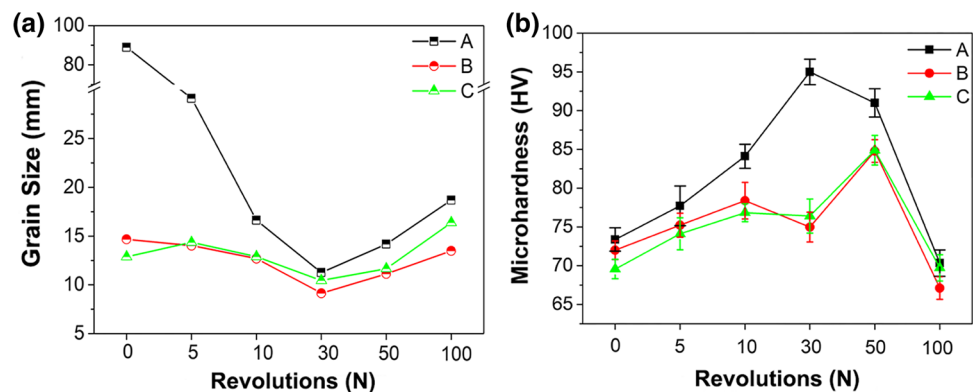
Fig. 13 The XRD patterns of AZ80 alloy during the CBE and RBE process

Fig. 14 **a** The average grain size and **b** the microhardness of the CBE and RBE samples at three different regions

deformation texture, which needs more in-depth research to explain this phenomenon.

5 Conclusions

As a new severe plastic deformation method, the RBE process can successfully produce high performance cylindrical tubes. The deformation characteristics of the AZ80 tubes processed by the RBE process has been studied through the FEM simulation and physical experiment. The conclusions are as follows:

1. The effective strain of the RBE process is higher than that of the CBE process, and the effective strain increases with the rotating revolutions increasing. The effective strain distribution of the tube inner wall changes from the "M" shape of the CBE samples to the "A" shape of the RBE samples, which can be attributed to the effect of additional rotation during the RBE process. Furthermore, the deformation uniformity of the sample also has been improved through the RBE process.
2. The large plastic strain can be obtained during the RBE process due to the cumulative plastic deformation caused by the continuous rotation of the open punch. The damage value increases with the rotating revolutions increasing. The extrusion load of the RBE process is lower than the CBE process and the maximum reduction of the FEM simulation and experimental results can reach 62.8% and 31.6%, respectively. The load reduction of the RBE process can be attributed to the change of the friction stress and the primary stress of the materials.
3. The RBE process can effectively refine the grains and improve the mechanical properties of the materials comparing with the CBE process. The minimum average grain size is obtained in 30 N sample at the three regions of A, B and C, and the values are 11.26 μm, 9.14 μm, and 10.45 μm, respectively. Moreover, the maximum decrease in the average grain size of the RBE process relative to the CBE process can reach 90% at the region A of the 30 N sample. In addition, the maximum microhardness values of the regions A, B and C are 98 HV at 30 N, 84.8 HV and 84.9 HV at 50 N.

References

1. Y. Estrin, A. Vinogradov, Acta Mater. **61**, 782 (2013)
2. T. Mungole, P. Kumar, M. Kawasaki, T.G. Langdon, J. Mater. Sci. **50**, 3549 (2015)
3. V.M. Segal, Mater. Sci. Eng. A **271**, 322 (1999)
4. G.S. Dyakonov, S. Mironov, I.P. Semenova, R.Z. Valiev, S.L. Semiatin, Acta Mater. **173**, 174 (2019)
5. B. Li, B.G. Teng, G.X. Chen, Mater. Sci. Eng. A **774**, 396 (2019)
6. Y. Saito, H. Utsunomiya, N. Tsuji, T. Sakai, Acta Mater. **47**, 579 (1999)
7. W. Habila, H. Azzeddine, B. Mehdi et al., Mater. Charact. **147**, 242 (2019)
8. A.P. Zhilyaev, G.V. Nurislamova, B.-K. Kim, M.D. Baró, J.A. Szpunar, T.G. Langdone, Acta Mater. **51**, 753 (2003)
9. W.T. Sun, X.G. Qiao, M.Y. Zheng et al., Acta Mater. **151**, 260 (2019)
10. S. Mizunuma, Mater. Sci. Forum **503–504**, 185 (2006)
11. W. Bochniak, A. Korbel, Mater. Sci. Technol. **16**, 664 (2000)
12. W. Bochniak, A. Korbel, J. Mater. Process. Technol. **134**, 120 (2003)
13. A. Korbel, W. Bochniak, Scr. Mater. **51**, 755 (2004)
14. A. Korbel, W. Bochniak, P. Ostachowski, L. Błaż, Metall. Mater. Trans. A **42**, 2881 (2011)
15. L.X. Kong, L. Lin, P.D. Hodgson, Mater. Sci. Eng. A **308**, 209 (2001)
16. X. Ma, M.R. Barnett, Y.H. Kim, Int. J. Mech. Sci. **45**, 1717 (2003)
17. X. Ma, M.R. Barnett, Y.H. Kim, Int. J. Mech. Sci. **46**, 449 (2004)
18. Q. Wang, Z.M. Zhang, J.M. Yu, Y. Xue, Procedia Eng. **207**, 383 (2017)
19. J.M. Yu, Z.M. Zhang, Q. Wang, H.Y. Hao, J.Y. Cui, L. Li, Mater. Lett. **215**, 195 (2018)
20. Y. Xue, Z.M. Zhang, Y.J. Wu, G. Lu, Adv. Mater. Res. **328–330**, 2394 (2011). https://doi.org/10.4028/www.scientific.net/AMR.328-330.2394
21. M. Costas, D. Morin, O.S. Hopperstad, T. Børvik, M. Langseth, J. Mech. Phys. Solids **123**, 190 (2019)
22. S. Fatemi-Varzaneh, A. Zarei-Hanzaki, Mater. Sci. Eng. A **504**, 104 (2009)
23. G. Faraji, H. Jafarzadeh, H. Jeong, M. Mashhadi, H. Kim, Mater. Des. **35**, 251 (2012)
24. X.S. Xia, Q. Chen, Z.D. Zhao, M.L. Ma, X.G. Li, K. Zhang, J. Alloys Compd. **623**, 62 (2015)
25. N. Tsuji, B.L. Li, Mater. Sci. Forum **539–543**, 2837 (2007)
26. L.S. Toth, C. Gu, Mater. Charact. **92**, 1 (2014)
27. R. Pippan, F. Wetscher, M. Hafok, A. Vorhauer, I. Sabirov, Adv. Eng. Mater. **8**, 1046 (2006)
28. T. Hebesberger, H.P. Stüwe, A. Vorhauer, F. Wetscher, R. Pippan, Acta Mater. **53**, 393 (2005)
29. R. Pippan, S. Scheriau, A. Taylor, M. Hafok, A. Hohenwarter, A. Bachmaier, Annu. Rev. Mater. Res. **40**(1), 319 (2010). https://doi.org/10.1146/annurev-matsci-070909-104445
30. C. Xu, K. Xia, T.G. Langdon, Acta Mater. **55**, 2351 (2007)
31. J.H. Li, F.G. Li, C. Zhao, H. Chen, X.K. Ma, J. Li, Mater. Sci. Eng. A **656**, 142 (2016)